Microfluidic Ultrasonic Shaker

Junjun Lei,[1,2,*] Feng Cheng,[1,2] Gaokun Zheng,[1,2] and Li Lin[1,2]

[1] *State Key Laboratory of Precision Electronic Manufacturing Technology and Equipment, Guangdong University of Technology, Guangzhou 510006, China*

[2] *School of Electromechanical Engineering, Guangdong University of Technology, Guangzhou 510006, China*

(Received 7 May 2022; revised 5 August 2022; accepted 3 October 2022; published 4 November 2022)

We report on a wave-driven microfluidic ultrasonic shaker that can stably trap and oscillate microparticles in water in a microchannel. The microfluidic ultrasonic shaking system mainly consists of a microfluidic chip and two orthogonally excited piezoelectric transducers: one for creating radiation force potential wells for three-dimensional trapping of microparticles and the other for generating sound destabilization to shake the trapped microparticles. It is shown that two standing waves of different but close frequencies provide a shaking force [approximately $F_0\cos(2\pi\,\Delta f t)$, with F_0 and Δf being the force amplitude and the frequency difference, respectively] that can repeatedly perturb a trapped microparticle and cause it to execute spontaneous oscillations. The dynamic behavior of microparticle oscillation driven by two sound waves is found to be equivalent to a forced harmonic oscillator (i.e., a mass on a spring) that has been extensively described in the literature. Specifically, experiments at various ultrasonic excitations show that the oscillating frequency of a stably trapped microparticle is determined by the frequency difference between the two sound waves, and the shaking amplitude scales inversely to the frequency difference and is affected by pressure amplitudes of both sound waves. We foresee that the illustrative microfluidic ultrasonic shaker presented here opens perspectives for dynamic manipulation of single microparticles or clusters in microscale acoustofluidic systems.

DOI: 10.1103/PhysRevApplied.18.054013

I. INTRODUCTION

Noncontact manipulation of particles using resonant ultrasonic fields is a rapidly growing research field that is receiving increasing attention in fields of physics, biology, medicine, and chemistry [1–4]. When a resonant ultrasonic field is established in an acoustofluidic device, the movements of particles suspended in the fluid medium are determined by two main acoustic forces, i.e., the acoustic radiation force (ARF) and the acoustic streaming (AS) induced drag force. In many cases, the ARF is the main engine for particle manipulation while the AS effect is regarded as a disturbance as it usually places a lower limit on the particle size that can be manipulated by the ARFs [5]. Diverse particle manipulations including patterning [6–9], focusing [10–13], separation [14–16], and transportation [17–20] enabled by ARFs have been demonstrated.

In ultrasonic particle manipulation devices where resonant ultrasonic fields are established, particles are driven towards positions where the radiation force potential is a minimum [21]. In general, solid or liquid particles that contribute to a positive acoustic contrast factor experience net ARF towards the pressure nodes, where they become trapped. Meanwhile, it is also known that a trapped particle could execute spontaneous oscillations around its equilibrium position when the cavity is detuned by exciting at a frequency that is just off resonance. The oscillation motion, in contrast to stable levitation, is referred to as oscillational instability [22], which has been frequently observed in midair single-axis acoustic levitators. Plenty of studies [23–27] have shown that, when a midair single-axis acoustic levitator is detuned at a certain off-resonance frequency, the oscillatory motion of a stably trapped particle is equivalent to a damped harmonic oscillator where the ARFs (and a drag force from the air) continuously drag the particle towards its equilibrium position.

While acoustic levitation of millimetric particles and their dynamics in midair acoustic levitators have been widely studied in the literature [28–30], little work has yet been conducted on ultrasonic oscillation of microscale objects in a microfluidic channel. To build a microfluidic ultrasonic shaker, an important first step is to realize stable three-dimensional (3D) acoustic trapping of microparticles. A number of papers have demonstrated 3D acoustic trapping of microparticles using different methods, such as single-beam acoustical trap [31] and standing waves [32], to create 3D force potential wells. Compared with

*junjun.lei@gdut.edu.cn

the standing wave configuration, the single-beam acoustical trap has a selectivity of a high spatial resolution down to the cell scale [33,34]. However, introducing sound instabilities in such systems for the investigation of ultrasonic microparticle oscillations is not trivial.

In this article, we propose and demonstrate an ultrasonic shaker enabled by acoustic microfluidics. 3D acoustic trapping and oscillation of single microparticles in a microchannel under various ultrasonic excitations are demonstrated and characterized. The dynamics of particle oscillation in this microfluidic ultrasonic shaker is found to be equivalent to a driven damped harmonic oscillator.

II. EXPERIMENTAL MEASUREMENTS

The acoustomicrofluidic device, shown schematically in Fig. 1(a), mainly consists of a glass capillary (Quartz, ZCQ), whose cross section is circular (diameter 0.9 mm) inside and square (1.5×1.5 mm^2) outside, and two piezoelectric transducers (PZTs, $40 \times 1.4 \times 1$ mm^3). See also Fig. S1 in the Supplemental Material [35] for the layout of the cross section of the acoustofluidic device. In a fluid channel of circular cross section, large microparticles can be focused to the channel center under the combining effects of ARF and AS-induced drag force when a (1, 0) mode is generated in the cross section of the channel [36]. Based on this principle, Lei *et al.* [11] demonstrated a highly efficient two-dimensional concentration of microparticles in a continuous flow in a similar acoustofluidic system to that shown in Fig. 1. Here, in a static fluid, as depicted in Fig. 1(a), microparticles are stably trapped in the channel, which is also in the z direction, by lateral resonances established along the channel, enabling 3D trapping. Merits of the geometric design can also be found from the Supplemental Material [35]. Owing to device symmetry, the 3D acoustic trapping can be achieved from an actuation of either of the PZTs. The performance of microparticles in the microchannel is imaged by a fluorescent microscope. Measurements of the microparticle oscillations are performed using the experimental arrangement that is schematically presented in Fig. 1(b). As shown, two 67.5° right triangular prims are placed between the chip and the objective lens, which can provide simultaneous imaging of the x-z and y-z planes of the channel and keep their real sizes, as also demonstrated previously by Lei *et al.* [37]. The acoustofluidic device and the prisms are compressed in a well-designed chip holder.

The whole experimental procedure is as follows. (i) Distilled water containing fluorescent spherical polystyrene particles (Fluoresbrite® microspheres, Polysciences) of 25 μm diameter with a deviation of ± 2.5 μm (manufacturer information) is introduced into the glass capillary by a 20-ml syringe pump. (ii) The focus planes of the microscope are adjusted to simultaneously image $x = 0$ and $y = 0$ (where microparticles are supposed to be trapped) by

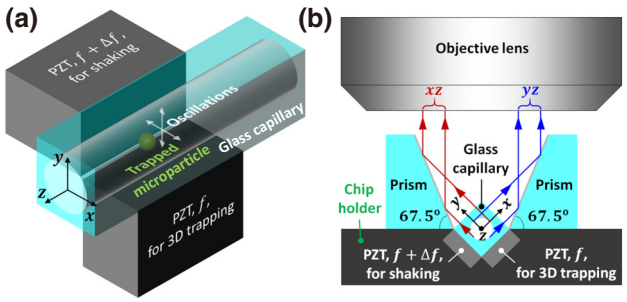

FIG. 1. Schematic of a microfluidic ultrasonic shaker. (a) The acoustic microfluidic system, which mainly consists of a glass capillary and two piezoelectric transducers (PZTs), one for three-dimensional trapping and the other for shaking of microparticles; (b) principle of simultaneous imaging of ultrasonic microparticle oscillations in x-z and y-z planes of the microchannel.

positioning horizontal and vertical stages. (iii) 3D acoustic trapping of single microparticles (diluted) is achieved by actuating one of the PZTs at frequency f. (iv) The trapped microparticle is then exposed to another sound wave at frequency $f + \Delta f$ that is actuated from the other PZT. Interference between the two sound waves creates a shaking force field for the trapped microparticle and causes it to oscillate at driving-dependent frequencies, Δf, and with amplitudes, A. (v) The shaking of single microparticles under various ultrasonic actuations is recorded for further analysis. Here, both PZTs (Pz4, COSSON) are driven by sinusoidal signals, which are generated by a functional generator (AFG1062, Tektronix), amplified by a dual-channel power amplifier (DPA2698, JUNTEK), and monitored by an oscilloscope (TBS1102B, Tektronix). The microparticle's position in each video frame is monitored using a Huawei P40 Pro cell phone (equipped with Leica Quad Camera) at 60 frames/s and processed by Zootracer [38].

The 3D acoustic trapping, shown in Fig. 2(a), is achieved with an actuation of one PZT at $f = 1.044$ MHz; at this frequency, microparticles in the microchannel are firstly focused to the channel axis by acoustic forces under the effects of the cross-section (1, 0) resonant mode and then trapped to their nearest acoustic kinematic energy density maxima by lateral acoustic forces in the z direction of the channel (see also a video in the Supplemental Material [35]). The trapped microparticles are forced into spontaneous oscillations when the second PZT is actuated at $f + \Delta f$ (with $0.01 < \Delta f < 20$ Hz here). It is found that the microparticles are oscillating in 3D space [owing to the imaging method described in Fig. 1(b)], which is different to the case seen in a typical midair single-axis acoustic levitator where a trapped particle generally oscillates only in the standing wave direction [39]. The trajectory of a 3D trapped microparticle for a detuning frequency $\Delta f = 0.6$ Hz is shown in Figs. 2(b)–2(d), where the x and

y oscillations are plotted. It can be seen that the oscillating trajectory of the trapped microparticle in the y direction is not strictly a harmonic motion, but presents a slightly distorted pattern, which may be attributed to the more complicated force distribution in the presented system than in a single-axis acoustic levitator. A discrepancy between the amplitudes of these two oscillations is observed, due to different strengths of the two PZTs. For the oscillations presented in Fig. 2(b), it can be seen that ξ_x and ξ_y are approximately $\pi/2$ out of phase, and the microparticle traces out a pearlike trajectory in the cross section of the channel, as plotted in Fig. 2(d). Experiments in various acoustofluidic devices and of various ultrasonic excitations show that the trajectory of microparticle oscillation in the x-y plane is not related to Δf but is affected to some extent by the combination of driving voltages of the two transducers. It is worth noting that, in the experiments, stable oscillations (with no decay) are observed immediately after the second PZT is detuned (with $\Delta f \neq 0$), indicating that the transient time that a trapped microparticle takes to reach stable oscillation from rest is negligible.

To show the performance of microfluidic ultrasonic shaking in more detail, we further investigate how the microparticle oscillations are related to the key parameters (including mainly the detuning frequencies Δf and the driving voltages $V_{\text{p.p.}}$) of the ultrasonic actuations. The periodicity of microparticle oscillation is measured at various driving conditions. It can be seen from Fig. 3(a) that the measured frequency (f) that a trapped microparticle oscillates at scales linearly with the detuning frequency Δf, while the driving amplitudes seem to have no influence on the oscillating frequency [see Fig. S4(a) in the Supplemental Material [35]]. However, all the ultrasonic parameters mentioned previously are shown to affect the oscillating amplitude of a trapped microparticle. With an increase of Δf, the oscillating amplitude decreases rapidly (close to a negative power function) and can hardly be distinguished when $\Delta f > 15$ Hz, as plotted in Fig. 3(b). Meanwhile, as expected, higher driving voltages can induce stronger ARFs on microparticles, which can not only achieve faster trapping, but can also enable larger amplitude oscillations. Examples with varying peak-to-peak voltages ranging from 6 to 26 V can be found from Fig. S4 in the Supplemental Material [35].

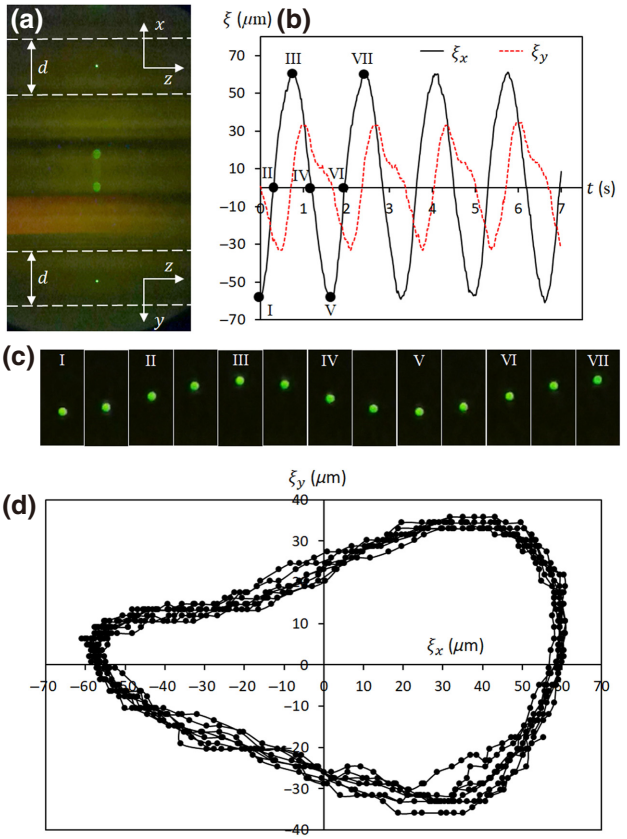

FIG. 2. Ultrasonic trapping and oscillation of a single microparticle in a microchannel. (a) Three-dimensional acoustic trapping of a spherical polystyrene particle 25 μm in diameter, where $d = 0.9$ mm indicates the channel diameter; (b) oscillating displacements (ξ) of a trapped microparticle at a detuning frequency $\Delta f = 0.6$ Hz, where both x and y oscillations (ξ_x and ξ_y, respectively) are plotted; (c) consecutive images showing the microparticle oscillation in the x direction; and (d) plot of the trajectory of the microparticle shaking in the cross section of the channel. A video showing the acoustic trapping and oscillation of a single microparticle in this microfluidic ultrasonic shaker can be found from the Supplemental Material [35].

III. THEORETICAL MODEL

The 3D trapped microparticle's oscillating displacement from its rest or equilibrium position in any direction, e.g., $\xi(t)$, may be solved from the equation of motion for a damped harmonic oscillator driven by a harmonic force field, that is,

$$m_p' \frac{d^2\xi}{dt^2} + c\frac{d\xi}{dt} + s\xi = Fe^{i\omega t}, \tag{1}$$

where $m_p' = m_p + m_p(\rho_f/2\rho_p)$ represents the "virtual mass" of a microparticle with m_p, ρ_f, and ρ_p being the particle mass, fluid density, and particle density, respectively; c is the mechanical resistance, s is the stiffness, and F is the amplitude of the driving force for oscillation. Here, the damping mainly comes from the viscous drag during microparticle oscillation. s and F, derived in the following, may be determined from the ARF field. The AS-induced drag force is ignored here as it is generally much smaller than the ARF on a microparticle of 25 μm in diameter in such a system [36].

For a small spherical microparticle in an acoustical field in a viscous fluid, the Reynolds number in the system may be considered sufficiently low that the viscous drag on the particle can be assumed as a linear force (following Stokes'

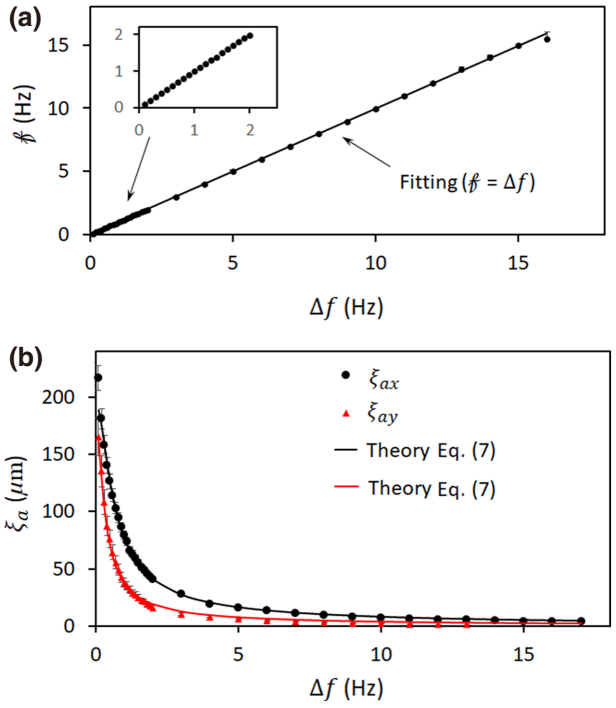

FIG. 3. Characterizations of the microparticle shaking at various detuning frequencies, Δf. (a) The measured oscillating frequency, $\not\!\!f$; and (b) the measured oscillating amplitude ξ_a, where ξ_{ax} and ξ_{ay} indicate the x and y components, and the error bars indicate the discrepancies observed in multiple measurements. Both driving voltages remain unchanged. The solid lines in (b) show the values calculated from Eq. (7).

law [40]), $\mathbf{F}_d = -6\pi\mu r\mathbf{v}$, where μ is the dynamic viscosity of the fluid, r is the particle radius, and $\mathbf{v}$ is the particle velocity. The mechanical resistance in Eq. (1) is then $c = -6\pi\mu r$, which is applicable for small Reynolds numbers ($\mathrm{Re} = 2\rho_f r|\mathbf{v}|/\mu$) and assumes that history forces are negligible.

Methods for calculating the ARF acting on a spherical particle have been described by various authors [41–46]. Here, in standing wave fields, the ARF vector field is well approximated by the Gorkov potential [43] (assuming the particle is small compared to the acoustic wavelength, valid for the cases considered in this work),

$$\mathbf{F}_{\mathrm{rad}} = -\nabla U, \tag{2}$$

$$U = \frac{4\pi r^3}{3}\left[\left(1 - \frac{\rho_f c_f^2}{\rho_p c_p^2}\right)\overline{E_{\mathrm{pot}}} - \frac{3(\rho_p - \rho_f)}{2\rho_p + \rho_f}\overline{E_{\mathrm{kin}}}\right], \tag{3}$$

where c_p and c_f are the sound speed in particle and fluid, $\overline{E_{\mathrm{kin}}} = \rho_f|\mathbf{u}_1|^2/4$ ($\mathbf{u}_1$ is the first-order acoustic velocity in fluid) and $\overline{E_{\mathrm{pot}}} = |p_1|^2/(4\rho_f c_f^2)$ (p_1 is the first-order acoustic pressure) are the time-averaged kinematic and potential energy density. Here, the total acoustic pressure is the sum of the two sound waves, that is, $p_1 = p_1^{\mathrm{tr}} + p_1^{\mathrm{os}}$, with each component being given by $p_1^{\mathrm{tr}} = p_0^{\mathrm{tr}}\sin(k^{\mathrm{tr}}y)e^{i\omega^{\mathrm{tr}}t}$ and $p_1^{\mathrm{os}} = p_0^{\mathrm{os}}\sin(k^{\mathrm{os}}x)e^{i\omega^{\mathrm{os}}t}$, where p_0 is the pressure amplitude, k is the wavenumber, ω is the angular frequency, the superscripts tr and os represent trapping and oscillating, respectively, and $\omega^{\mathrm{os}} - \omega^{\mathrm{tr}} = \Delta\omega = 2\pi\Delta f$. The relationship between the first-order acoustic velocity and pressure satisfies the linearized Euler's equation, $\rho_0\partial\mathbf{u}_1/\partial t + \nabla p_1 = 0$, which gives $\mathbf{u}_1 = i\nabla p_1/\rho_f\omega$.

Substituting the acoustic pressure and velocity fields into the Gorkov equation, the resulting ARF components become (see Supplemental Material [35] for more information)

$$F_{\mathrm{rad},x} = -\frac{\pi r^3}{3\rho_f c_f^2}k^{\mathrm{os}}p_0^{\mathrm{os}}\cos(k^{\mathrm{os}}x)[p_0^{\mathrm{os}}\sin(k^{\mathrm{os}}x) + p_0^{\mathrm{tr}}\sin(k^{\mathrm{tr}}y)\cos(2\pi\Delta ft)], \tag{4}$$

$$F_{\mathrm{rad},y} = -\frac{\pi r^3}{3\rho_f c_f^2}k^{\mathrm{tr}}p_0^{\mathrm{tr}}\sin(k^{\mathrm{tr}}y)[p_0^{\mathrm{tr}}\cos(k^{\mathrm{tr}}y) + p_0^{\mathrm{os}}\sin(k^{\mathrm{os}}x)\cos(2\pi\Delta ft)]. \tag{5}$$

It can be seen that, in this wave-driven microfluidic ultrasonic shaking system, both the second terms in the x and y components of the ARF contain a time-dependent term $\cos(2\pi\Delta ft)$, which is the main engine for shaking and can cause a microparticle to execute spontaneous oscillation in both directions at frequency Δf, as observed in the experiments [e.g., Fig. 2(b)]. Without the time-dependent term, the stable part of the ARF can only result in stable microparticle trapping. It can be known from Eqs. (1), (4), and (5) that the first terms in the ARF equations contribute to the stiffness of the system, which gives $s = \pi r^3 k^2 p_0^2/(3\rho_f c_f^2)$ (using $\sin(k\xi) \approx k\xi$ for a small shaking displacement, i.e., $k\xi \ll 1$). It is worth noting that, as shown in Fig. 2 and the video in the Supplemental Material [35], the demonstrated microparticle oscillations in the z direction are far weaker than the oscillations in the other directions, and thus only the x and y components of the ARF are of interest here.

The complex expressions for ARFs (i.e., the restoring or driving force for oscillation) make it difficult to find an analytical solution of Eq. (1), which, however, could be simplified at certain circumstances. Assuming that a microparticle oscillates with a small displacement ξ (e.g., x and y), where $\cos(k\xi) \approx 1$ and $\sin(k\xi) \approx k\xi$, and the coordinate of the microparticle in the other direction can be considered constant when calculating its oscillation in one direction, the equation of motion of a trapped microparticle in the ξ direction can further be approximated to the following form,

$$\frac{d^2\xi}{dt^2} + \gamma\frac{d\xi}{dt} + \omega_0^2\xi = F_0\cos(2\pi\Delta ft). \tag{6}$$

In this classical equation, according to the properties of water ($\rho_f = 1000\ \mathrm{kg/m^3}$, $c_f = 1500\ \mathrm{m/s}$) and polystyrene particles ($\rho_p = 1050\ \mathrm{kg/m^3}$, $c_p = 1962\ \mathrm{m/s}$), the key parameters are determined: $\gamma = c/m'_p \approx 4.1 \times 10^3$ is the damping coefficient; ω_0, the natural frequency of the particle in the detuned trap, is found by $\omega_0 = 2\pi f_0 = \sqrt{s/m'_p} \approx \sqrt{1.2 \times 10^{-6} p_0^2}$, which depends on the amplitude of the driving pressure; and $F_{0,} = -k^{\mathrm{os}} k^{\mathrm{tr}} p_0^{\mathrm{os}} p_0^{\mathrm{tr}} \xi_0 / (6\rho_p \rho_f c_f^2)$ is a part of the ARF with ξ_0 being the initial or equilibrium position of the microparticle, which is related to the pressure amplitudes of both sound waves. In the absence of gravity, the ARF tends to locate a microparticle at the channel axis (without detuning frequency). Taking gravity into account, a microparticle could be stably trapped at a slightly lower position (see also Fig. S2 in the Supplemental Material [35]), where a balance between the ARF and gravity is obtained. It is worth noting that expressions for ω_0 and F_0, described previously, hold true for oscillations in both x and y directions.

Equation (6) describes the approximated equation of motion for a 3D trapped microparticle in this microfluidic ultrasonic shaker, which is equivalent to a mass on a spring driven by a harmonic force that has been extensively described in the literature. The steady oscillation has a general solution, i.e., $\xi(t) = \xi_a \cos(\omega t - \theta)$, where $\omega = \Delta\omega = 2\pi\,\Delta f$ [which can explain the detuning frequency-dependent oscillation frequency (i.e., $= \Delta f$) observed in experiments, as shown in Fig. 3(a)] and

$$\xi_a = \frac{F_0}{\sqrt{(\Delta\omega)^2\gamma^2 + \left[(\Delta\omega)^2 - \omega_0^2\right]^2}}. \tag{7}$$

Figure 4 plots the relationship between the dimensionless oscillation amplitude, $\overline{\xi_a} = \xi_a/\xi_{a0}$ (with $\xi_{a0} = F_0/\omega_0^2$ being the oscillation amplitude at $\Delta\omega = 0$), and the dimensionless detuning frequency, $\bar{f} = \Delta\omega/\omega_0 = \Delta f\,/f_0$, at various acoustic pressure amplitudes p_0 (assuming that $p_0^{\mathrm{tr}} = p_0^{\mathrm{os}} = p_0$). It can be seen that the response of oscillation amplitude to the detuning frequency varies at different acoustic pressure amplitudes. At low pressure levels, ξ_a monotonically decreases with the increase of Δf. When the acoustic pressure amplitude rises to above around 5 MPa, the oscillation amplitude tends to firstly grow with Δf and then fall with a further increase of Δf after reaching its maximum at $\Delta f\,/f_0 \approx 1$. Thus, for a normal acoustic pressure amplitude of 0.05–0.5 MPa in a typical acoustic microfluidic device such as presented here, ξ_a tends to monotonically decrease with increasing Δf, which is consistent with the experimental measurements. In Fig. 3(b) we see that the measured oscillating amplitudes compare well with the theoretical values calculated from Eq. (7) [parameters (with units) used for calculations: ξ_{ax}, $F_0 = 2.4$ N and $\omega_0 = 111.4$ rad/s; ξ_{ay}, $F_0 =$ 1.1 N and $\omega_0 = 78.7$ rad/s]. The agreement between the experimental measurements and the theoretical values proves that the linear model is a good approximation of this wave-driven microfluidic ultrasonic shaker. However, when analyzing large-amplitude oscillations at high pressure amplitudes, the nonlinearity may have to be considered and a nonlinear model might be necessary [47].

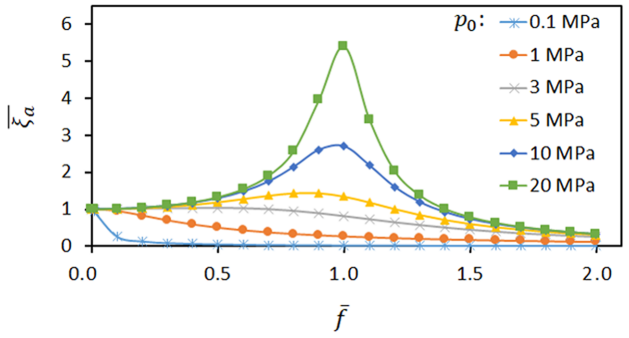

FIG. 4. Relationship between the dimensionless oscillating amplitude, $\overline{\xi_a}$, and the dimensionless detuning frequency, $\bar{f}$, at different acoustic pressure amplitudes, p_0.

IV. CONCLUDING DISCUSSION

In summary, we propose here a microfluidic ultrasonic shaker enabled by acoustofluidics. It is shown that two standing waves of different but close frequencies can generate a periodic shaking force that can stably oscillate a 3D trapped microparticle in a microfluidic channel at a frequency equal to their frequency difference Δf and at a constant amplitude without decay, determined by Δf and the acoustic pressure amplitudes p_0. The microparticle oscillation is not limited to a one-dimensional motion that is usually seen in midair acoustic levitators. In a regular acoustofluidic microparticle and cell manipulation device where the acoustic pressure amplitude is typically $p_0 <$ 1 MPa [48], the oscillating amplitude tends to monotonically decrease with the increase of Δf. At much higher pressure amplitudes, where the nonlinear acoustic effect should be involved, the linear model presented in Eq. (1) might not be enough to characterize the accurate motion of microparticles in such a microfluidic ultrasonic shaker and a full solution of the microparticle acoustophoresis may be required.

It is anticipated that more diverse microfluidic ultrasonic shakers could be built up from different configurations of ultrasonic excitations (e.g., single vortex beam systems [33]) and designs of microfluidic chips. Upon a deeper understanding of particle dynamics in microfluidic ultrasonic shakers, the reported system opens up the practical dynamic manipulation of single microparticles or clusters in microacoustofluidic systems. Frequency-detuning-induced single-axis oscillation has been demonstrated to

have influences on the organization of multiparticle systems [49,50]; the presented microfluidic ultrasonic shaker introduces a new mechanism for controlling interparticle interactions in a microfluidic environment, which may also create opportunities for the assembly of colloids with desired micro- or nanostructures [51]. Controlled oscillation of microparticle clusters also has potential in biological applications, e.g., tissue engineering, where oscillatory fluid shear forces have been shown to be advantageous for the culture of cell aggregates [52].

ACKNOWLEDGMENTS

This research has been funded by the National Natural Science Foundation of China (Grant No. 11804060); the Natural Science Foundation of Guangdong Province (Grant No. 2021A1515010244); the Guangzhou Basic and Applied Basic Research Foundation (Grant No. 202102020414); and the Guangdong University of Technology.

[1] B. W. Drinkwater, Dynamic-field devices for the ultrasonic manipulation of microparticles, Lab Chip **16**, 2360 (2016).
[2] A. Ozcelik, J. Rufo, F. Guo, Y. Gu, P. Li, J. Lata, and T. J. Huang, Acoustic tweezers for the life sciences, Nat. Methods **15**, 1021 (2018).
[3] M. Baudoin and J.-L. Thomas, Acoustic tweezers for particle and fluid micromanipulation, Annu. Rev. Fluid Mech. **52**, 205 (2020).
[4] G. Liu, J. Lei, F. Cheng, K. Li, X. Ji, Z. Huang, and Z. Guo, Ultrasonic particle manipulation in glass capillaries: a concise review, Micromachines **12**, 876 (2021).
[5] H. Bruus, J. Dual, J. Hawkes, M. Hill, T. Laurell, J. Nilsson, S. Radel, S. Sadhal, and M. Wiklund, Forthcoming Lab on a Chip tutorial series on acoustofluidics: Acoustofluidics-exploiting ultrasonic standing wave forces and acoustic streaming in microfluidic systems for cell and particle manipulation, Lab Chip **11**, 3579 (2011).
[6] J. Lei, Formation of inverse Chladni patterns in liquids at microscale: roles of acoustic radiation and streaming-induced drag forces, Microfluid. Nanofluid. **21**, 50 (2017).
[7] D. J. Collins, R. O'Rorke, C. Devendran, Z. Ma, J. Han, A. Neild, and Y. Ai, Self-Aligned Acoustofluidic Particle Focusing and Patterning in Microfluidic Channels from Channel-Based Acoustic Waveguides, Phys. Rev. Lett. **120**, 074502 (2018).
[8] G. T. Silva, J. H. Lopes, J. P. Leão-Neto, M. K. Nichols, and B. W. Drinkwater, Particle Patterning by Ultrasonic Standing Waves in a Rectangular Cavity, Phys. Rev. Appl. **11**, 054044 (2019).
[9] J. Lei, F. Cheng, G. Liu, K. Li, and Z. Guo, Dexterous formation of unconventional Chladni patterns using standing bulk acoustic waves, Appl. Phys. Lett. **117**, 184101 (2020).
[10] A. Fornell, F. Garofalo, J. Nilsson, H. Bruus, and M. Tenje, Intra-droplet acoustic particle focusing: simulations and experimental observations, Microfluid. Nanofluid. **22**, 75 (2018).
[11] J. Lei, F. Cheng, K. Li, and Z. Guo, Two-dimensional concentration of microparticles using bulk acousto-microfluidics, Appl. Phys. Lett. **116**, 033104 (2020).
[12] Z. Li, P. Li, J. Xu, W. Shao, C. Yang, and Y. Cui, Hydrodynamic flow cytometer performance enhancement by two-dimensional acoustic focusing, Biomed. Microdevices **22**, 27 (2020).
[13] M. S. Gerlt, A. Paeckel, A. Pavlic, P. Rohner, D. Poulikakos, and J. Dual, Focusing of Micrometer-Sized Metal Particles Enabled by Reduced Acoustic Streaming via Acoustic Forces in a Round Glass Capillary, Phys. Rev. Appl. **17**, 014043 (2022).
[14] A. Lenshof and T. Laurell, Continuous separation of cells and particles in microfluidic systems, Chem. Soc. Rev. **39**, 1203 (2010).
[15] M. Wu, A. Ozcelik, J. Rufo, Z. Wang, R. Fang, and T. Jun Huang, Acoustofluidic separation of cells and particles, Microsyst. Nanoeng. **5**, 32 (2019).
[16] J. Lei, F. Cheng, K. Li, and Z. Guo, Numerical simulation of continuous separation of microparticles in two-stage acousto-microfluidic systems, Appl. Math. Model. **83**, 342 (2020).
[17] N. Bjelobrk, D. Foresti, M. Dorrestijn, M. Nabavi, and D. Poulikakos, Contactless transport of acoustically levitated particles, Appl. Phys. Lett. **97**, 161904 (2010).
[18] P. Glynne-Jones, C. E. Demore, C. Ye, Y. Qiu, S. Cochran, and M. Hill, Array-controlled ultrasonic manipulation of particles in planar acoustic resonator, IEEE Trans. Ultrason. Ferroelectr. Freq. Control **59**, 1258 (2012).
[19] D. Foresti, M. Nabavi, M. Klingauf, A. Ferrari, and D. Poulikakos, Acoustophoretic contactless transport and handling of matter in air, Proc. Natl. Acad. Sci. U. S. A. **110**, 12549 (2013).
[20] C. Yoon, B. J. Kang, C. Lee, H. H. Kim, and K. K. Shung, Multi-particle trapping and manipulation by a high-frequency array transducer, Appl. Phys. Lett. **105**, 214103 (2014).
[21] M. Hill and N. R. Harris, in *Microfluidic Technologies for Miniaturized Analysis Systems*, edited by S. Hardt and F. Schönfeld (Springer, Boston, MA, US, 2007), pp. 357.
[22] J. Rudnick and M. Barmatz, Oscillational instabilities in single-mode acoustic levitators, J. Acoust. Soc. Am. **87**, 81 (1990).
[23] N. Pérez, M. A. B. Andrade, R. Canetti, and J. C. Adamowski, Experimental determination of the dynamics of an acoustically levitated sphere, J. Appl. Phys. **116**, 184903 (2014).
[24] M. A. B. Andrade, T. S. Ramos, F. T. A. Okina, and J. C. Adamowski, Nonlinear characterization of a single-axis acoustic levitator, Rev. Sci. Instrum. **85**, 045125 (2014).
[25] S. Tsujino, Y. Sato, Y. Takeda, and T. Tomizaki, Oscillation resonances and anisotropic damping of the motion of acoustically levitated droplets in single-axis acoustic levitators, Appl. Phys. Lett. **115**, 053702 (2019).
[26] M. A. B. Andrade, S. Polychronopoulos, G. Memoli, and A. Marzo, Experimental investigation of the particle oscillation instability in a single-axis acoustic levitator, AIP Adv. **9**, 035020 (2019).
[27] A. Dolev, S. Davis, and I. Bucher, Noncontact Dynamic Oscillations of Acoustically Levitated Particles by Parametric Excitation, Phys. Rev. Appl. **12**, 034031 (2019).

[28] M. A. B. Andrade, N. Pérez, and J. C. Adamowski, Review of progress in acoustic levitation, Braz. J. Phys. **48**, 190 (2018).
[29] M. A. B. Andrade, A. Marzo, and J. C. Adamowski, Acoustic levitation in mid-air: Recent advances, challenges, and future perspectives, Appl. Phys. Lett. **116**, 250501 (2020).
[30] M. A. Abdelaziz and D. G. Grier, Dynamics of an acoustically trapped sphere in beating sound waves, Phys. Rev. Res. **3**, 013079 (2021).
[31] D. Baresch, J.-L. Thomas, and R. Marchiano, Observation of a Single-Beam Gradient Force Acoustical Trap for Elastic Particles: Acoustical Tweezers, Phys. Rev. Lett. **116**, 024301 (2016).
[32] S. Yang, Z. Tian, Z. Wang, J. Rufo, P. Li, J. Mai, J. Xia, H. Bachman, P.-H. Huang, M. Wu, C. Chen, L.P. Lee, and T. J. Huang, Harmonic acoustics for dynamic and selective particle manipulation, Nat. Mater. **21**, 540 (2022).
[33] Z. Gong and M. Baudoin, Three-Dimensional Trapping and Dynamic Axial Manipulation with Frequency-Tuned Spiraling Acoustical Tweezers: A Theoretical Study, Phys. Rev. Appl. **16**, 024034 (2021).
[34] Z. Gong and M. Baudoin, Single beam acoustical tweezers based on focused beams: A numerical analysis of 2D and 3D trapping capabilities, arXiv:2205.10033 (2022).
[35] See Supplemental Material at http://link.aps.org/supplemental/10.1103/PhysRevApplied.18.054013 for more information.
[36] J. Lei, F. Cheng, and K. Li, Numerical simulation of boundary-driven acoustic streaming in microfluidic channels with circular cross-sections, Micromachines **11**, 240 (2020).
[37] J. Lei, F. Cheng, K. Li, G. Liu, Y. Zhang, Z. Guo, and Y. Zhang, Simultaneous imaging and manipulation of microparticles in horizontal and vertical planes of microchannels using a single objective lens, Appl. Phys. Lett. **117**, 224101 (2020).
[38] Zootracer, (Microsoft Research) https://www.microsoft.com/en-us/research/project/zootracer/
[39] T. Fushimi, T. L. Hill, A. Marzo, and B. W. Drinkwater, Nonlinear trapping stiffness of mid-air single-axis acoustic levitators, Appl. Phys. Lett. **113**, 034102 (2018).
[40] G. G. Stokes, On the effect of the internal friction of fluids on the motion of pendulums, Trans. Cambridge Philos. Soc. **9**, 8 (1851).
[41] L. V. King, On the acoustic radiation pressure on spheres, Proc. R. Soc. London **A147**, 212 (1934).
[42] K. Yosioka and Y. Kawasima, Acoustic radiation pressure on a compressible sphere, Acustica **5**, 167 (1955).
[43] L. P. Gor'kov, On the forces acting on a small particle in an acoustical field in an ideal fluid, Sov. Phys. Dokl. **6**, 773 (1962).
[44] H. Bruus, Acoustofluidics 7: The acoustic radiation force on small particles, Lab Chip **12**, 1014 (2012).
[45] I. D. Toftul, K. Y. Bliokh, M. I. Petrov, and F. Nori, Acoustic Radiation Force and Torque on Small Particles as Measures of the Canonical Momentum and Spin Densities, Phys. Rev. Lett. **123**, 183901 (2019).
[46] A. A. Doinikov, M. S. Gerlt, and J. Dual, Acoustic Radiation Forces Produced by Sharp-Edge Structures in Microfluidic Systems, Phys. Rev. Lett. **124**, 154501 (2020).
[47] L. E. Kinsler, A. R. Frey, A. B. Coppens, and J. V. Sanders, *Fundamentals of Acoustics*, 4th ed. (Wiley, New York, 2000).
[48] M. Ohlin, I. Iranmanesh, A. E. Christakou, and M. Wiklund, Temperature-controlled MPa-pressure ultrasonic cell manipulation in a microfluidic chip, Lab Chip **15**, 3341 (2015).
[49] M. X. Lim, A. Souslov, V. Vitelli, and H. M. Jaeger, Cluster formation by acoustic forces and active fluctuations in levitated granular matter, Nat. Phys. **15**, 460 (2019).
[50] B. Drinkwater, An ultrasonic shake-up, Nat. Phys. **15**, 423 (2019).
[51] H. Sazan, S. Piperno, M. Layani, S. Magdassi, and H. Shpaisman, Directed assembly of nanoparticles into continuous microstructures by standing surface acoustic waves, J. Colloid Interface Sci. **536**, 701 (2019).
[52] U. S. Jonnalagadda, M. Hill, W. Messaoudi, R. B. Cook, R. O. C. Oreffo, P. Glynne-Jones, and R. S. Tare, Acoustically modulated biomechanical stimulation for human cartilage tissue engineering, Lab Chip **18**, 473 (2018).